Excited-State Geometry Method for Calculation of the Absolute Resonance Raman Cross Sections of the Aromatic Amino Acids

John F. Gaff and Stefan Franzen*

Department of Chemistry, North Carolina State University, Raleigh, North Carolina 27695

Received: October 24, 2008; Revised Manuscript Received: March 9, 2009

The time correlator formalism was used to calculate the absolute resonance Raman cross sections for the aromatic amino acids based on density functional theory calculations of the ground-state potential energy surfaces combined with projection along normal mode eigenvectors in the excited state. The geometric difference between the minima of the ground and excited states along each normal mode was calculated to provide inputs for the time correlator in the linear approximation. The calculated dimensionless nuclear displacements, Δ_i, provide the electron−phonon coupling constants, $S_i = \Delta_i^2/2$, for the corresponding Raman active mode of frequency ω_t. The method is generally applicable to molecules that are Franck−Condon active. As an example we have chosen to calculate the absolute resonance Raman cross sections of models of the aromatic amino acids phenylalanine, tyrosine, and tryptophan. We discuss the role played by substituents on the aromatic ring that decrease vibronic activity to a level that permits application of the time correlator. While the method may have limitations for molecules of high symmetry, the current study of excited-state displacements and electronic structure indicates that the $L_{a,b}$ states are Franck−Condon active in the aromatic molecules studied.

Introduction

Vibrational spectroscopy offers an avenue for the study of structure that provides specific information on the chemical environment of amino acids, nucleic acids, and other biological cofactors.[1−10] Resonance Raman spectroscopy has a significant advantage over infrared and nonresonant Raman spectroscopy in that it gives the ability to tune the scattering wavelength to specific chromophores or classes of amino and nucleic acids. The resonance effect provides a method for selectively observing the vibrations of the molecules that absorb at the excitation wavelength with little or no contribution from the remaining molecules in the system, permitting simplification of experimentally determined vibrational spectra. Resonance Raman spectroscopy is specifically of interest for the study of the aromatic amino acids (phenylalanine, tyrosine, tryptophan) of proteins in order to measure dynamic motions of proteins. The vibrational assignments for the peaks in the experimental resonance Raman spectra of the aromatic rings within these acids are based on studies of the model systems benzene, toluene, and pyrrole.[11−13] However, the calculation of resonance Raman intensities has presented a challenge due to the intrinsic involvement of excited states in the scattering process.

The calculation of Raman intensities from first principles has been approached using two methods. In the first method, the Raman scattering intensities are obtained from the gradient of excited state calculated by *ab initio* molecular orbital theory. In the second method, *ab inito* calculations of the excited-state geometry have been used to obtain geometric displacements with respect to the ground state that can serve as the input for transform theory[14] or for the time correlator.[15,16] The first approach has been widely used because of the availability of derivatives in quantum chemistry packages such as Gaussian.[17] The calculation of analytic derivatives in quantum chemistry is a well-established method both in Hartree−Fock[18,19] and in density functional theory (DFT).[20,21] While the calculation of infrared intensities based on the dipole derivative is relatively accurate, polarizabilities are notoriously difficult to calculate. The method is applicable in the linear approximation and then only in the limit of small excited-state displacements. Moreover, the polarizability derivative approach is most frequently used as a nonresonant Raman approach and has only recently been applied to resonant Raman scattering.[21] Recent studies have also used the approach to estimate the resonance enhancement in surface enhanced Raman scattering (SERS).[22,23] The second approach, involving explicit calculation of excited-state displacements, has application when the geometry change in the excited state is large. However, since there are no *ab initio* packages that incorporate the time correlator method, the method has been used infrequently.[15,16]

We have taken the initial steps toward a practical method that permits time-dependent (TD)-DFT calculations to be combined with the time correlator method for the calculation of absolute resonance Raman scattering cross sections. The method described in this work is based on explicit calculation of the excited-state geometry change along each normal mode using the DFT code DMol,[3,24] to provide the linear coupling term, S_j, for the jth normal mode of frequency ω_j, which serves as input for the calculation of the Raman cross section using the time correlator approach.[25−27] Herein, we present an excited-state geometry method for calculation of the intensities of the Raman bands of the three aromatic amino acids commonly observed in the resonance Raman spectra of proteins. The calculated results were compared to the available spectral data obtained for the aromatic amino acids.[1,4,10,28−38]

Methods

The time correlator method for calculation of resonance Raman cross sections uses the excited-state displacement and

* Author to whom correspondence should be addressed. Phone: 919−515−8915. E-mail: Stefan_Franzen@ncsu.edu.

10.1021/jp809431k CCC: $40.75 © 2009 American Chemical Society
Published on Web 04/10/2009

vibrational frequency as inputs. The excited-state geometry method is based on explicit calculation of potential energy minimum along each normal mode obtained from a vibrational frequency calculation in the harmonic approximation. The transition moment required for calculation of the absolute resonance Raman cross section is obtained from the absorption spectrum. The damping is obtained from an estimate of the homogeneous line width of the absorption spectrum. The calculation of each of these parameters is detailed in the following.

The generalized gradient approximation of Perdew and Wang,[39] Burke−Lee−Yang−Parr (BLYP), and Perdew−Burke−Ernzerhof (PBE)[40] density functional are employed in the ground-state energy calculations as implemented by the electronic structure package DMol^3 using a double numeric basis set with one polarization function.[24,41] Optimized geometries were obtained using the conjugate gradient method constrained to an energy difference of less than 5×10^{-6} hartree. Excited-state transitions were determined by employing the time-dependent (TD)-DFT as implemented in the DFT package ORCA.[42] In order to achieve a comparable level of accuracy, the (TD)-DFT calculations were carried out using Ahlrich's double-ζ basis set with one polarization function.[43−45] The numerical and analytic basis sets used in DMol^3 and ORCA, respectively, are comparable in that both are double-ζ with a single polarization function. Calculations were carried out on a Parallel Quantum Solutions QS8-2800C QuantumCube. Following geometry optimization, the Hessian matrix or force constant matrix was constructed by finite differences of the analytical gradient, with the finite differencing proceeding from atom to atom. The potential energy distribution (PED) for each mode was determined by the contribution of the internal coordinates (stretches, bends, and torsions) to the normal coordinates. The PED for vibrational modes was determined using the program fcart01 written by Collier.[46]

The dimensionless nuclear displacement, Δ, was then calculated for each normal mode in the optimized structure. This was accomplished by projection along each of the *i* normal mode coordinates, Q_k, by the creation of explicit structures derived from the eigenvectors in Cartesian coordinates, Δx_k, Δy_k, and Δz_k. In order to verify that the modes contained a minimum, the nuclear displacements, Q, were calculated for 11 geometries ranging from 1 to −1 in mass weighted atomic units ($Q_j = -1$, $-4/5$,..., 0,..., $+4/5$, $+1$). The displaced structure, representing the excited state for each respective mode, was found by taking the geometry optimized Cartesian coordinate for each respective atom and subtracting the mass weighted normal mode eigenvector for each respective displacement step

$$C_j = \left(\frac{\Delta q_j}{M_{\mathrm{W}}^{1/2}}\right)\left(\frac{Q_j}{0.529\ 167}\right) \tag{1}$$

$\Delta q_j = \Delta x_j$, Δy_j, and Δz_j, C is the excited-state structure, and M_{w} is the molecular weight of the corresponding atom. The displacement ranges over the values that map out the motions of each normal mode. The ground and excited potential energy surfaces were calculated using single-point energy calculations on each displaced structure. Potential energy surfaces were then fitted to a fourth-order polynomial. Using this fitting function, the minima along each mode was obtained analytically. The difference between the minima of both the ground and excited states determined the magnitude of the nuclear displacement along that normal mode. The dimensionless displacement along the *i*th normal mode, Δ_i, was calculated by dividing the normal mode displacement by the rms displacement, $1/(2\alpha_i)^{1/2}$, where α_i is the displacement of the excited from the ground state and the conversion factor $(2\pi^2 m_{\mathrm{p}} c)/(10^{20}\ \mathrm{h})$ was employed to convert the energy to wavenumbers. A threshold of $S_i = 0.05$ for the electron−phonon coupling constant was used. Any S_i value below this number was neglected in the two-time correlator calculation. The two-time correlator implemented in the program TIMETHERM, developed by Shreve and Mathies,[25] was used to calculate absorption spectra and Raman excitation profiles (REPs) at 300 K for both the forbidden L_{a-b} and the allowed B_{ab} bands. In the two-time correlator formalism, the resonance Raman scattering cross section, σ_{R}, can be expressed as

$$\sigma_{\mathrm{R}} = \frac{(8\pi\omega_{\mathrm{s}}^3\omega_{\mathrm{o}}M_{if}^4)}{(9\hbar^2c^4)}\left(\int_0^\infty \langle f|i(t)\rangle\ \exp\{i(\omega_i+\omega_{\mathrm{o}})t-\Gamma t\}\ \mathrm{d}t\right)^2 \tag{2}$$

where M_{if} is the transition moment of the molecule, ω_{o} is the frequency of incident radiation, ω_{s} is the frequency of scattered radiation, ω_i is the vibrational quantum in the ground state, and Γ is the damping constant. TIMETHERM is based upon a Franck−Condon model (A-term scattering)[47] for the coupling of the vibrational modes to the electronic structure. The B-term scattering (Herzberg−Teller and Jahn−Teller) is not taken into account in this model. The absorption cross section, σ_{A}, is given by

$$\sigma_{\mathrm{A}} = \frac{(2\pi\omega_{\mathrm{o}}M_{if}^2)}{(3\hbar c)}\int_{-\infty}^{\infty} \langle i|i(t)\rangle\ \exp\{i(\omega_i+\omega_{\mathrm{o}})t-\Gamma t\}\ \mathrm{d}t \tag{3}$$

The damping constant, Γ, provides a homogeneous broadening term. The Lorentzian line shapes that result from eqs 2 and 3 are convolved with a Gaussian function to represent inhomogeneous broadening. The contributions of homogeneous and inhomogeneous line broadening were estimated based on fits to experimental absorption spectra.

Transition moments for the forbidden $L_{a,b}$ bands were determined by integration of the experimental absorption band

$$(M_{if})^2 = \left(\frac{6909c\varepsilon_{\mathrm{o}}\hbar}{\pi N_{\mathrm{A}}}\right)\int_{\mathrm{band}} \frac{\varepsilon(\nu)}{\nu}\,\mathrm{d}\nu \tag{4}$$

ϵ is the molar extinction coefficient in units of $\mathrm{M}^{-1}\ \mathrm{cm}^{-1}$, ν is wavenumber in units of cm^{-1}, c is the speed of light, and ϵ_{o} is the permittivity of a vacuum constant. Due to the paucity of data for the electronic absorption spectrum for the allowed transitions of the four models, transition moments for the B_{ab} bands were estimated using a TD-DFT calculation.

The calculations were carried out within the harmonic approximation. However, there are important observed vibrations that have splitting due to Fermi resonance. It is possible to identify overtones and combination bands by searching the calculated modes for an energy match between combinations of modes $\nu_j + \nu_k$ with an allowed mode ν_i, with a defined threshold, $\Delta\nu$. Typically the threshold was set at $\Delta\nu = 5\ \mathrm{cm}^{-1}$.

$$\Delta\nu = \nu_i - (\nu_j + \nu_k) \tag{5}$$

where $\nu_i = 1$,..., $3N-6$, $\nu_j = \nu_i$,..., $3N-6$, and $\nu_k = \nu_j$,..., $3N-6$.

Results and Discussion

Toluene, *para*-cresol, and 3-methylindole (3MI) were studied as models of the aromatic amino acids phenylalanine, tyrosine, and tryptophan, respectively. Structures for each model are displayed in Figure 1. Based on the TD-DFT calculations, the

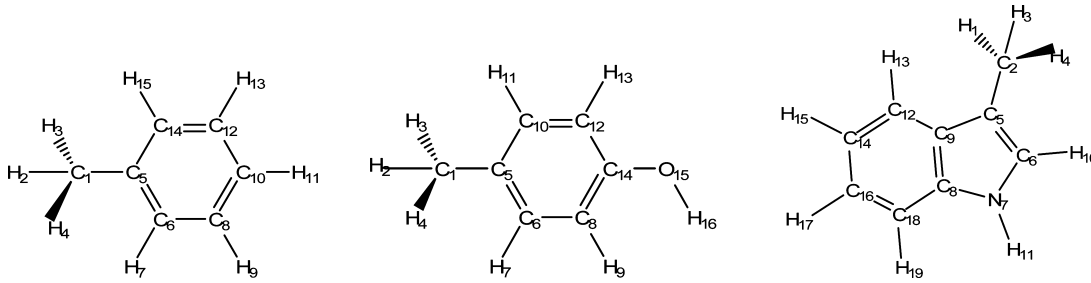

Figure 1. Structures of aromatic amino acid models, toluene, *para*-cresol, and 3-methylindole (3MI).

TABLE 1: Electronic Transitions Selected for Calculation of Excited-State Normal Mode Displacements[a]

molecule	transition	observed Raman wavelengths (nm)
toluene	25 → 28	192, 200, 218, and 220
toluene	25 → 27	244
para-cresol	27 → 30	192 and 200
para-cresol	29 → 31	218 and 244
3MI	35 → 37	218 and 229
3MI	35 → 36	244 and 260

[a] These transitions were calculated using the TD-DFT method (ORCA).[42]

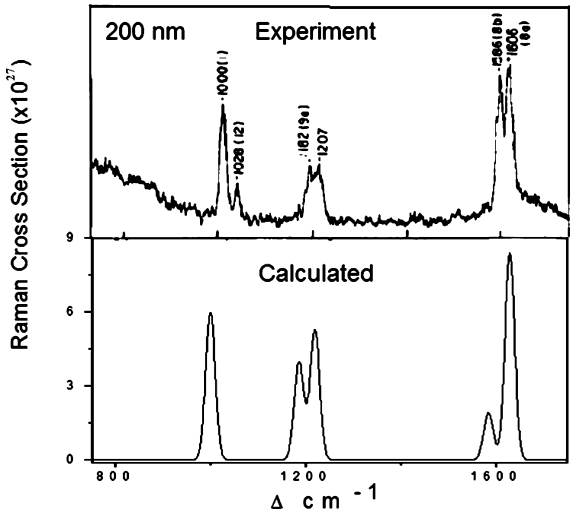

Figure 2. Calculated and experimental[32] resonance Raman spectrum for toluene, excited in preresonance with the B_{ab} transition for phenylalanine, based on the active modes presented in Table 2. Calculated cross sections are scaled by a factor of 10.[27]

transitions with the greatest contribution were identified and used for the excited-state normal mode projections and for the calculation of Raman cross sections for both the allowed and forbidden bands. These transitions are presented in Table 1. For all three molecules, the REP and absorption spectra have roughly the same line shape, which is expected for a Franck−Condon active transition with small excited-state nuclear displacements and line broadening that is approximately as large as the mode frequency. Calculated REPs presented in this study are displayed for only the modes for which comparable experimental data are available. All of the major vibrational modes are accounted for in the analysis, meaning that the agreement is excellent between the predicted and observed Raman active modes. For the amino acid models, these modes consist only of the Raman bands corresponding to the aromatic ring modes. These modes have been studied extensively using UV resonance Raman spectroscopy in the laboratory, providing a wealth of experimental data.[1,2,8,28,29,32,33,35,36,48−51] Complete sets of REPs can be found in the Supporting Information. Comparison of experimental and calculated REPs along with calculated resonance Raman spectra were carried out in pre/resonance with the totally allowed $B_{a,b}$ and the quasi-forbidden $L_{a,b}$ transitions, with wavelengths extracted from refs 1 and 31.

Table 2 gives the calculated and experimental frequencies, along with electron−phonon coupling constants for the three molecules employed in this study. For example, six Raman active modes were determined for toluene based on the magnitude of the excited-state displacement, Δ_i. Figure 2 shows resonance Raman spectrum at an excitation wavenumber of 50 000 cm^{-1} (200 nm) based upon these active modes, which serve as a model for phenylalanine. The resonance Raman spectrum was calculated at an excitation wavelength of 192 and 200 nm in resonance with the allowed $B_{a,b}$ transitions and 218, 220, and 244 nm, pre/resonant with the forbidden $L_{a,b}$ transitions of phenylalanine. Figure 3 displays the REPs for toluene. For *para*-cresol, both the resonance Raman spectrum and excitation profiles were calculated for the same transitions as for toluene. Figure 4 shows the calculated resonance Raman spectrum for *para*-cresol, and Figure 5 displays three relevant REPs. 3MI exhibits a more complex resonance Raman spectrum compared to that of toluene or *para*-cresol due to the addition of the pyrrole ring. The resonance Raman spectrum displayed in Figures 6 is based upon the 11 active modes found for 3MI, with the resonance Raman spectrum calculated at an excitation wavelength of 218 nm. The REPs for 3MI are shown in Figure 7.

The sum of the normal mode displacements for modes of frequency ω_i, weighted by Δ_i, gives the overall geometry of the excited state. The excited-state geometry changes have some common features for the aromatic amino acids. The C(5)−CH_3 bond of the methyl group contracts in all of the excited states. The $B_{a,b}$ and $L_{a,b}$ excited states have either an alternating pattern of contraction and elongation or a slightly asymmetric ring expansion, respectively. The excited state for the $B_{a,b}$ transition toluene has an asymmetric geometry change reported in Table 2 of the Supporting Information. There is an expansion for the four carbons not bound to the C(5) carbon (Figure 1). The $L_{a,b}$ transition has a more symmetric expansion of the ring. The $L_{a,b}$ transition of *para*-cresol exhibits an expansion of all bonds except C(5)−C(6) and C(12)−C(14), which are opposite one another on the ring (Figure 1). The $B_{a,b}$ transition has a similar pattern of contraction and elongation of ring bonds with a slight elongation of the C(14)−O(15) bond. The $B_{a,b}$ transition of 3MI also has a ring geometry that has an alternating pattern of expansion and compression of the bonds. The $L_{a,b}$ transition exhibits a more uniform expansion of the ring.

In the following we consider some of the detailed mode assignments needed to compare the experimental and calculated Raman cross sections and excitation profiles. While these comparisons can be seen in Table 4, the experimental and calculated spectra have been calculated at appropriate excitation wavelengths in Figures 2, 4, and 6 for phenylalanine, tyrosine,

TABLE 2: Calculated Frequencies and Electron−Phonon Couplings for Allowed Transitions for the Three Molecular Models of the Aromatic Amino Acids

toluene			para-cresol			3-methylindole		
mode	PBE	*S*	mode	PBE	*S*	mode	PBE	*S*
1	105.1		1	41.4		1	149.4	
2	221.9		2	113.1		2	170.0	
3	346.2		3	208.8		3	189.1	
4	412.3		4	293.3		4	236.1	
5	493.8		5	326.5		5	284.9	
6	524.5		6	417.4		6	403.2	
7	631.6		7	424.1		7	439.2	
8	712.7		8	460.7		8	468.2	
9	748.0		9	505.1		9	529.8	
10	791.9		10	647.2		10	561.8	
11	853.4		11	701.8		11	563.7	
12	907.2		12	735.4		12	575.1	
13	967.3		13	782.2		13	689.8	
14	978.3		14	813.5		14	701.7	
15	989.3		15	844.1	1.607	15	718.1	
16	998.5	0.401	16	901.2		16	736.6	0.065
17	1035.6	0.113	17	940.1		17	760.6	0.164
18	1042.7		18	962.3		18	810.0	
19	1091.7		19	1016.0		19	870.8	0.132
20	1158.8		20	1028.0		20	889.0	
21	1184.8	0.206	21	1108.7		21	940.7	
22	1218.0	0.263	22	1159.0		22	975.1	
23	1325.4		23	1173.8	0.114	23	1021.3	0.414
24	1350.2		24	1212.0	0.512	24	1028.8	
25	1369.9		25	1264.4		25	1076.0	
26	1429.6		26	1312.3		26	1086.4	
27	1443.8		27	1351.6		27	1124.8	
28	1466.8		28	1368.8		28	1160.9	
29	1506.0		29	1421.5		29	1219.8	0.150
30	1583.1	0.065	30	1438.4		30	1252.3	0.120
31	1627.8	0.242	31	1457.8		31	1293.4	0.068
32	2957.3		32	1518.6		32	1343.3	0.065
33	3024.4		33	1600.1	0.754	33	1369.3	
34	3050.4		34	1634.8	0.973	34	1382.6	
35	3110.1		35	2952.9		35	1417.3	
36	3113.1		36	3016.5		36	1442.0	
37	3133.0		37	3047.2		37	1456.4	
38	3161.4		38	3095.5		38	1465.6	
39	3180.3		39	3109.8		39	1489.2	0.065
			40	3126.1		40	1546.2	0.329
			41	3132.0		41	1572.6	0.184
			42	3728.9		42	1641.2	
						43	2957.8	
						44	3016.1	
						45	3089.2	
						46	3103.8	
						47	3120.6	
						48	3141.2	
						49	3164.3	
						50	3231.9	
						51	3604.8	

and tryptophan, respectively, in order to make the comparisons more evident. The REPs are presented in Figures 3, 5, and 7, respectively. All calculated modes are assigned using the notation used in prior studies for the respective molecules.

Toluene. The resonance Raman spectrum and REPs for toluene, calculated with a transition lengths of 0.86 and 0.11 Å for the allowed and forbidden transitions, are displayed in Figures 2 and 3, respectively. Table 4 lists experimental Raman cross section values[29,30,34,35] in resonance with the $B_{a,b}$ at 192 and 200 nm as well as pre/resonance with L_a and L_b transitions at excitation wavelengths of 218, 220, and 244 nm. The REP in Figure 3 shows two distinct peaks corresponding to two transitions observed in toluene. The largest scattering cross section is observed in resonance with the allowed $B_{a,b}$ transition at wavelengths lower than 200 nm, with a maximum at approximately at 180 nm. The vibronically allowed L_b transition has a maximum wavelength of 263 nm. Five prominent peaks are discernible at 999, 1185, 1218, 1583, and 1628 cm^{-1} in the calculated resonance Raman spectrum for 200 nm excitation shown in Figure 3. Mode ν_{12} at 999 cm^{-1} corresponds to the trigonal ring breathing mode of the monosubstituted aromatic ring, seen experimentally at 1006 cm^{-1}.[1,10] Modes ν_{8a} and ν_{8b} are of in-plane ring deformations, experimentally observed at 1586 and 1606 cm^{-1}. Two additional modes of similar intensity, ν_{18a} and ν_{9a}, are observed at 1185 and 1218 cm^{-1}, respectively. These modes consist of in-plane C−H bending, corresponding to the experimental values of 1182 and 1207 cm^{-1} for phenylalanine.[1,10]

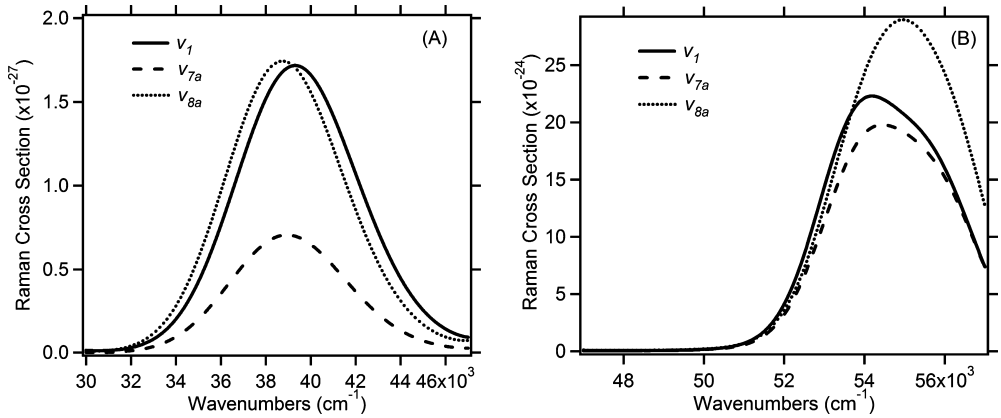

Figure 3. Calculated REPs for three of the most intense Raman bands of toluene. (A) Excitation profiles coinciding with the forbidden transition, $M = 0.11$ Å, $E_{0-0} = 37\,000$ cm^{-1}, $\sigma = 100$ cm^{-1}, and $\Gamma = 2200$ cm^{-1}. (B) Profiles coinciding with the B_{ab} transition of toluene, $M = 0.86$ Å, $E_{0-0} = 54\,000$ cm^{-1}, $\sigma = 350$ cm^{-1}, and $\Gamma = 1100$ cm^{-1}.

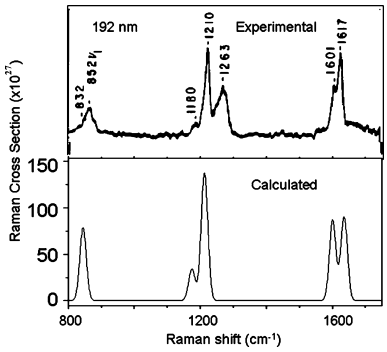

Figure 4. Calculated and experimental[34] resonance Raman spectrum of *para*-cresol based on the active modes presented in Table 2. Calculated cross sections are scaled by a factor of 10.[27]

Figure 3 shows that there is reasonable agreement of the calculated and experimental resonance Raman spectra for excitation at 200 nm. The experimental and calculated Raman cross sections of ν_{8a} for 200 nm excitation are $\sigma_R = 0.257 \times 10^{-24}$ and 0.211×10^{-24} cm^2/(mol-str), respectively. Similar agreement with experiment is found for the 999 cm^{-1} mode, ν_{12}, whose cross sections are $\sigma_R = 0.209 \times 10^{-24}$ and 0.150×10^{-24} cm^2/(mol-str), for the experimental and calculated values, respectively. The three modes at 1185, 1218, and 1583 cm^{-1}, ν_{9a}, ν_{7a}, and ν_{8b}, have scattering cross sections of $\sigma_R = 0.099 \times 10^{-24}$, 0.132×10^{-24}, and 0.049×10^{-24} cm^2/(mol-str), respectively. Of these only the ν_{8b} mode shows a disagreement of greater than 6% with experiment. The calculated value is 0.239×10^{-24} cm^2/(mol-str), which is about 5 times larger than the experimental value. We attribute this discrepancy to the vibronic character of this mode.

The cross sections for excitation at 192 nm, which is in resonance with the allowed $B_{a,b}$ transition, are also in reasonable agreement between theory and experiment. For modes ν_{12}, ν_{7a}, and ν_{8b}, experimental cross sections are $\sigma_R = 4.15$ and 3.60 ($\times 10^{-24}$), and 0.617×10^{-24} cm^2/(mol-str) respectively, compared to 4.00 and 3.03 ($\times 10^{-24}$), and 0.887×10^{-24} cm^2/(mol-str) from the calculations shown in Table 4. Mode ν_{8a} is the only outlier, with an experimental cross section of 0.519×10^{-24} and a calculated value of 4.11×10^{-24} cm^2/(mol-str), due to the vibronic character of the mode.

The model calculation presented here is only valid for Franck−Condon transitions. Modes which are enhanced when the Franck−Condon approximation breaks down, via B-term scattering, are not accounted for. While benzene is a molecule with a center of symmetry that has a number of nontotally symmetric modes, the addition of a methyl group to form toluene lowers the symmetry sufficiently that significant Franck−Condon character is introduced into the $L_{a,b}$ transitions.[1,30] This can be seen in the excited-state displacements shown in the Supporting Information. While benzene has a number of double-well minima in the excited state, symmetry breaking in toluene leads to a single minimum in these modes. Therefore, symmetry breaking leads to enhancement of nontotally symmetric modes in the Raman spectra. The lack of symmetry in the excited state can observed in the geometry given in Table 2 of the Supporting Information. For toluene the C(5)−CH_3 bond of the methyl group contracts, and the expansion of the ring is asymmetric with an expansion for the four carbons not bound to the C(5) carbon (see Figure 1). This asymmetric excited-state geometry change can be contrasted with benzene, which has a symmetric expansion of the ring. Since the method applied here is valid only for Franck−Condon active modes, the effect of symmetry lowering is to increase the number of modes that can be accurately calculated. For example, upon examination of the excitation wavelength at 244 nm, in preresonance with the L_b transition, it can be seen that the experimental and calculated cross sections are in accord with one another. For modes ν_{12}, ν_{7a}, and ν_{8b}, experimental cross sections are $\sigma_R = 2.80$, 1.20, and 2.50 ($\times 10^{-27}$) cm^2/(mol-str), respectively. The calculated cross sections of these modes are 1.83, 0.800, and 0.520 ($\times 10^{-27}$) cm^2/(mol-str), respectively. As was the case for resonance with the $B_{a,b}$ transitions, the ν_{8b} mode has the strongest vibronic character and the relative discrepancy of a factor of ~5.

***para*-Cresol.** Figure 4 displays the calculated resonance Raman spectrum for *para*-cresol, employing a transition length of 0.51 Å, in resonance with the B_{ab} transition. The REPs for three of the five active modes for this transition and the forbidden L_b transition are displayed in Figure 5. Cross sections that coincided with the forbidden transitions were calculated with a transition length of 0.23 Å. As found for toluene, two peaks are observed in the excitation profiles for each active mode, one peak having a maximum at 192 nm and another having a maximum at 275 nm, coinciding with the B_{ab} and the L_b transitions, respectively. Table 4 lists the experimental cross section values for active modes at wavelengths in pre/resonance with the allowed transition at 193 nm, and the forbidden transitions at 223 and 275 nm. The greatest deviation between experiment and theory can be observed with ν_{7a} at 1264 cm^{-1}. This dominant feature of the experimental resonance Raman

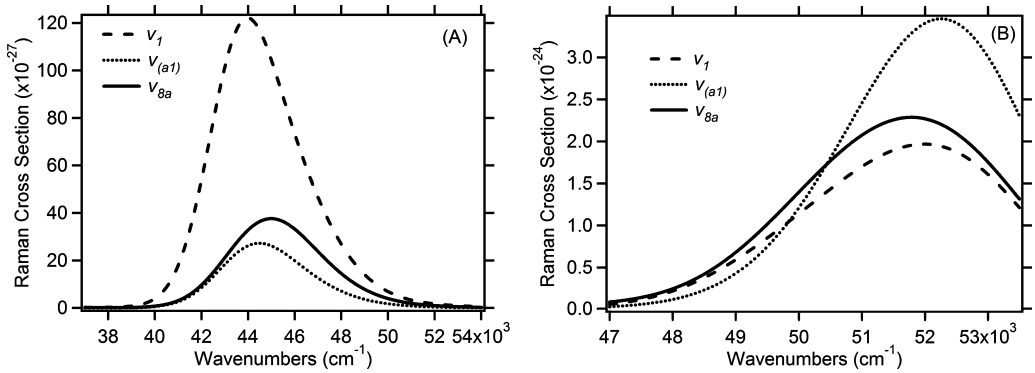

Figure 5. Calculated REPs for three of the most intense Raman bands of *para*-cresol. (A) Excitation profiles for the L_b transition of *para*-cresol, $M = 0.23$ Å, $E_{0-0} = 42\,000$ cm^{-1}, $\sigma = 30$ cm^{-1}, and $\Gamma = 1150$ cm^{-1}. (B) Excitations for the allowed, B_{ab} transition, $M = 0.51$ Å, $E_{0-0} = 49\,500$ cm^{-1}, $\sigma = 50$ cm^{-1}, and $\Gamma = 1100$ cm^{-1}.

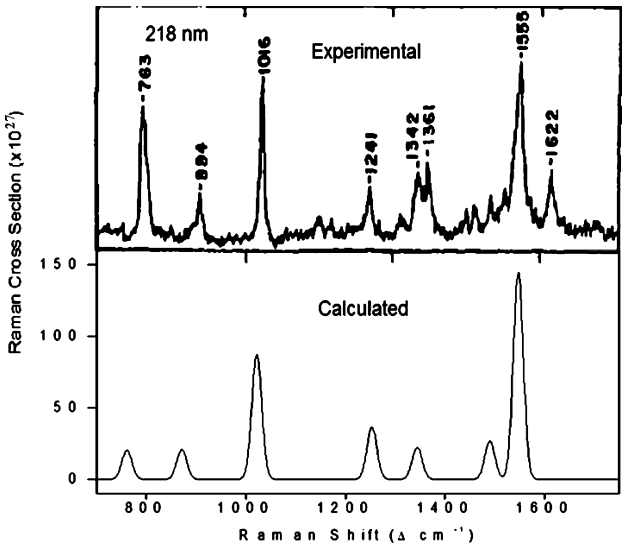

Figure 6. Calculated and experimental[33] resonance Raman spectrum for 3MI based on active modes in Table 2 in resonance with the $B_{a,b}$ transition. Calculated cross sections are scaled by a factor of 10.[27]

spectrum was calculated to also be at 1264 cm^{-1} and consists of a symmetric ring deformation with a large contribution arising from C−O stretching (20%).[30] Although excellent agreement is found between the experimental and calculated frequencies of this mode, the calculated intensity is nearly zero since ν_{7a} is a nontotally symmetric mode that is enhanced by vibronic coupling. Inspection of Figure 4 shows that the mode displaying the greatest Raman cross section is the totally symmetric para-substituted benzene stretch, ν_{a1}, observed at 1210 cm^{-1}.[11] This vibrational mode has a calculated Raman cross section of $\sigma_R = 3.43 \times 10^{-24}$ cm^2/(mol-str), which compares well to the experimental value of 4.11×10^{-24} cm^2/(mol-str). Mixing modes ν_{9a}, ν_{8a}, and ν_{8b} at 1175, 1601, and 1617 cm^{-1} gain intensity on resonance with the allowed $B_{a,b}$ transition.[52] The vibronic modes result from the mixing of the symmetry forbidden L_a and L_b electronic states with the $B_{a,b}$ state. Upon symmetry lowering of the benzene ring by substitution of a hydroxyl and methyl group, formerly vibronic modes gain Franck−Condon activity. Experimental cross sections for theses modes excited at 192 nm are $\sigma_R = 1.11$, 2.44, and 3.83 ($\times 10^{-24}$) cm^2/(mol-str)[34,53] and calculated values of $\sigma_R = 0.852$, 2.17, and 2.25 ($\times 10^{-24}$) cm^2/(mol-str), respectively.

Experimentally, the symmetric ring stretch, ν_1,[11] is observed as a doublet at 830 and 850 cm^{-1},[1] which is pH-dependent.[29] Tyrosinate is favored at high pH, but the splitting due to Fermi resonance with the overtone of ν_{16a} is observed at all pH values. The calculated value is a single band at 844 cm^{-1}, which lies exactly in between the peaks of the doublet at pH 6.0. The calculated scattering cross section of ν_1, $\sigma_R = 1.96 \times 10^{-24}$ cm^2/(mol-str), agrees with the experimental value of 2.12×10^{-24} cm^2/(mol-str). In preresonance with the $B_{a,b}$ transition at 200 nm, values for both theory and experimental are also in accord with one another (Table 4). The experimentally observed doublet is an important feature for experimental analysis of the hydrogen bonding environment of tyrosine.[5,10,33] Depending on the ratio of the relative intensities of the Fermi doublet peaks, the number of buried versus exposed tyrosine residues can be estimated.[10] A search using eq 5 indicated that the out-of-plane ring bending overtone ν_{16a} satisfies both the energetic and symmetry requirements to participate in the Fermi doublet. The first overtone of is $2\nu_{16a} = 832$ cm^{-1}, which is approximately equal to the frequency of ring breathing mode 841 cm^{-1},[34,52] in agreement with results presented elsewhere.[1,10,33,38] The symmetry of the first overtone is A_1 by definition, which permits coupling of the overtone with the fundamental ring breathing mode ν_1, which is also A_1.

3-Methylindole. Figures 6 and 7 show the resonance Raman spectrum and excitation profiles for 3MI, also known as skatole, calculated using transition lengths of 0.95 and 0.56 Å for the allowed and forbidden transitions, respectively. The excitation profiles show two distinct electronic transitions of 3MI at ∼212 nm and ∼303 nm, which correspond to the B_{ab} and L_b transitions. In the calculated Raman spectrum shown in Figure 6, there are two intense Raman bands at 1021 and 1546 cm^{-1}, with less intense peaks at 761, 877, 1252, 1343, and 1496 cm^{-1}. These modes are also prominent in the experimental resonance Raman spectra,[1,28,32,36] which exhibit strong Franck−Condon activity in the allowed $\pi \rightarrow \pi^*$ transition. As shown by the excitation profile in Figure 7, the peak with the greatest Raman cross section, a symmetric pyrrole and benzene in-plane ring mode corresponding to ν_{8a} in benzene is calculated to occur at a frequency of 1546 cm^{-1}. This mode is observed in the resonance Raman spectrum at 1555 cm^{-1}.[32] The calculated and experimental cross sections of this mode are $\sigma_R = 3.62$ and 2.00 ($\times 10^{-24}$) $\times 10^{-8}$ Å^2, respectively. The totally symmetric benzene and pyrrole in-phase ring breathing mode, ν_1, is calculated to occur at 761 cm^{-1}. Although the frequency of the mode is calculated accurately, the intensity of this mode shows the largest discrepancy between calculation and experiment, $\sigma_R = 0.510$ and 2.30 ($\times 10^{-24}$) cm^2/(mol-str), respectively. The mode at 1021 cm^{-1}, which is analogous to the toluene ν_{12} mode, shows much closer agreement with $\sigma_R = 1.55$ and 2.19 ($\times 10^{-24}$) cm^2/(mol-str) for calculation and experiment, respectively. The calculated mode at 1252 cm^{-1} is a pyrrole ring in-plane bending

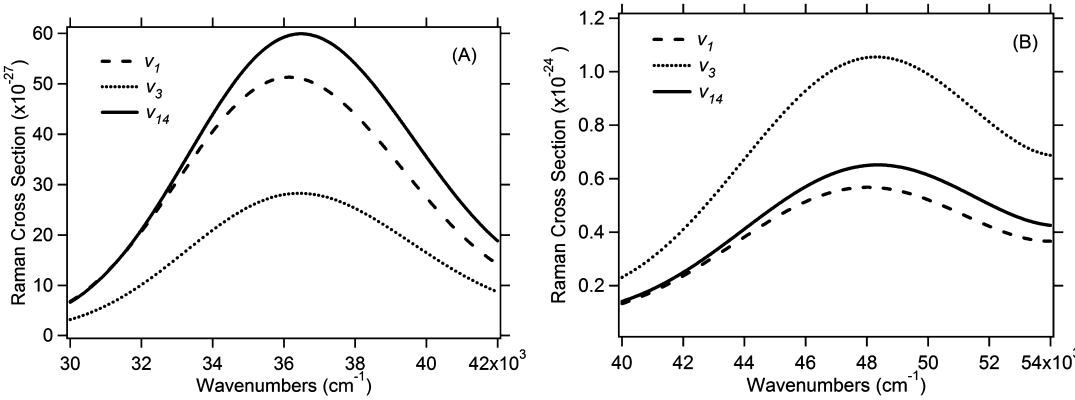

Figure 7. Calculated REPs for three of the most intense Raman bands of 3MI. (A) Excitation profiles for the L_b transition, $M = 0.56$ Å, $E_{0-0} = 33\,330$ cm^{-1}, $\sigma = 1500$ cm^{-1}, and $\Gamma = 2000$ cm^{-1}. (B) Excitation profiles for the allowed B_{ab} transition, $M = 0.95$ Å, $E_{0-0} = 44\,440$ cm^{-1}, $\sigma = 1000$ cm^{-1}, and $\Gamma = 3800$ cm^{-1}.

TABLE 3: Calculated and Experimental Resonance Raman Peak Comparison[a]

assignment	experimental (cm^{-1})	calculated (cm^{-1})	% difference
	toluene		
ν_{12}	1006	999	0.7
ν_{18a}	1031	1036	0.5
ν_{9a}	1187	1185	0.2
ν_{7a}	1212	1218	0.5
ν_{8a}	1604	1628	1.5
	para-cresol		
ν_1	835/854	844	1.2
ν_{9a}	1175	1174	0.1
ν_{a1}	1210	1211	0.1
ν_{7a}	1270	1264	0.5
ν_{8b}	1601	1600	0.1
ν_{8a}	1617	1635	1.1
	3MI		
ν_1	762	761	0.1
ν_{12}	1009	1021	1.2
ν_{9b}	1127	1125	0.2
ν_3	1220	1252	1.0
ν_{14}	1342/1360	1343	0.1/1.3
ν_{8a}	1555	1546	0.6
ν_{8b}	1578	1573	0.3

[a] Assignments are derived from the modes of benzene and toluene.[1,12,13,30]

with appreciable N−H bending and C−H bending on the benzene ring, observed at 1252 cm^{-1} in the experimental spectrum. The relatively small intensity of this mode is in agreement with the calculations, with $\sigma_R = 0.914$ and 0.374 ($\times 10^{-24}$) cm^2/(mol-str) for calculation and experiment, respectively. At 1343 cm^{-1}, ν_{14} is an in-plane benzene/pyrrole ring stretch, experimentally observed at 1342 cm^{-1}. This mode is the well-known Fermi doublet of tryptophan as discussed below. A complete set of percent differences between calculated and experimental frequencies for all models is given in Table 3.

The Raman cross sections for 3MI were compared with experimental data obtained in resonance with the B_{ab}, L_a, and L_b transitions at 217, 273, and 287 nm, respectively, in Table 4. Cross section values are in good agreement with excitation occurring at 218, 229, 244, and 260 nm. The greatest deviation between calculated and experimental data can be observed for the 1622 cm^{-1} vibration. Modes at 1460 and 1622 cm^{-1} fell below the threshold of $S = 0.0$ and are therefore not found to be Franck−Condon active by the calculation. In agreement between calculation and experiment, the mode at 1546 cm^{-1} shows the greatest amount of scattering at all excitation wavelengths from the calculations in pre/resonance with the $B_{a,b}$ transition. The experimental value of the scattering cross section, $\sigma_R = 2.00 \times 10^{-24}$ cm^2/(mol-str), compares reasonably well to the calculated value of 3.63×10^{-24} cm^2/(mol-str). The symmetric out-of-phase benzene and pyrrole breathing mode exhibits experimental cross sections of 1.55 and 0.494 ($\times 10^{-24}$) cm^2/(mol-str) at 218 and 229 nm, which agree quite well with the corresponding calculated values of $\sigma_R = 2.19$ and 1.52 ($\times 10^{-24}$) cm^2/(mol-str). The mode at 1622 cm^{-1} observed in the experimental spectrum of tryptophan is a vibronic mode, which means that the present method does not account for its scattering intensity.

The resonance Raman spectrum of tryptophan can also be correlated with protein environment based on the doublet at 1340−1360 cm^{-1}, which is known to be sensitive to both solvent effects and pH.[4,50,54,55] This Fermi doublet arises from a combination of a fundamental in-plane vibration and a combination of one or more out-of-plane vibrations. The sharpness and intensity of this line can be used as a diagnostic tool to determine whether or not the tryptophan residue is buried in the protein interior. Employing the same method used above for *para*-cresol, the fundamental and the combination bands composing the Fermi doublet were ascertained. The fundamental that constitutes part of the Fermi doublet is an in-plane stretch of the indole ring system observed at a frequency of 1343 cm^{-1}. Experimentally, this mode is observed in the region from 1342 to 1347 cm^{-1}.[4,52] Harada has suggested that the Fermi doublet of 3MI is a combination of the aforementioned fundamental and a combination band of two out-of-plane vibrations at 920 and 420 cm^{-1}, not an overtone.[4] Our calculations agree with this assessment. The fundamental, ν_{14}, at 1343 cm^{-1} can mix with bands arising from 941 and 403 cm^{-1}, both out-of-plane vibrations. The modes at 941 and 403 cm^{-1} are both of A″ symmetry, while the 1343 cm^{-1} mode is of A′ symmetry so that the symmetry requirements for the Fermi doublet are satisfied, A″ × A″ = A′. It is the of the out-of-plane vibrations, rather than the fundamental, that are the hydrogen bonding sensitive components. The PED for the mode at 403 cm^{-1} embodies an out-of-plane bend composed of H11−(N7−C6−C8), while at 941 cm^{-1} the PED contains all out-of-plane bends, consisting of 53% H15−(C14−C12−C16), 50% H17−(C16−C14−C18),13%H13−(C12−C9−C14),and8%H19−(C18−C8−C16). The in-plane fundamental ν_{14} consists of a 17% C9−C5 stretch, an 8% C12−C14−H15 bend, and 6% coming from both H13−C12−C14 and H15−C14−C16 bends. As can be seen in Table 4, the calculated scattering cross section of the tryptophan

TABLE 4: Comparison of Calculated and Experimental[1] Cross Sections for Toluene, *para*-Cresol, and 3MI

Toluene										
	Raman cross sections									
	192 nm[a]		200 nm[a]		218 nm[a]		220 nm[a]		244 nm[b]	
ν (cm^{-1})	exptl	calc	exptl	calc	exptl	calc	exptl	calc	exptl	calc
999	4.148	4.004	0.209	0.150	0.168	0.102	0.061	0.131	2.8	1.83
1030	n/a		n/a		n/a		0.029	0.040	0.5	0.4
1185	0.598	2.332	0.106	0.099	0.089	0.077	0.049	0.099	n/a	
1218	3.600	3.034	0.125	0.132	0.077	0.105	0.033	0.135	1.2	0.8
1583	0.617	0.887	0.239	0.049	0.128	0.049	n/a		n/a	
1628	0.519	4.110	0.257	0.211	0.311	0.165	0.176	0.210	2.5	0.52

para-Cresol								
	Raman cross section							
	192 nm[a]		200 nm[a]		218 nm[a]		244 nm[b]	
ν (cm^{-1})	exptl	calc	exptl	calc	exptl	calc	exptl	calc
844[c]	2.121	1.964	1.097	1.139	n/a		5	17.5
1180	1.113	0.852	0.801	0.283	0.213	0.210	12	4.6
1210	4.112	3.435	2.446	1.210	0.045	0.237	6	2.8
1264[d]	4.653	n/a	3.702	n/a	0.077	n/a	n/a	
1600	2.437	2.173	1.963	1.147	0.280	0.264	n/a	
1635	3.825	2.252	2.872	1.395	0.381	0.388	20	3.85

3-Methylindole								
	Raman cross section							
	218 nm[a]		229 nm[a]		244 nm[b]		260 nm[b]	
ν (cm^{-1})	exptl	calc	exptl	calc	exptl	calc	exptl	calc
761	2.301	0.507	0.550	0.356	10.0	27.9	50.0	32.6
877	0.406	0.521	0.172	0.365	4.0	n/a	n/a	n/a
1021	1.552	2.185	0.494	1.515	14.0	16.4	5.0	18.9
1125	n/a	n/a	n/a	n/a	5.0	30.3	n/a	n/a
1252	0.374	0.914	0.097	0.627	4.0	16.0	2.0	18.2
1343[c]	0.359	0.561	0.147	0.382	15.0	33.9	8.0	38.3
1360[c]	0.501		0.170		7.5		n/a	n/a
1460	0.419	n/a	0.077	n/a	5.5	n/a	6.0	n/a
1496	0.225	671	n/a	n/a	n/a	n/a	n/a	n/a
1546	2.003	3.625	0.598	2.446	18.0	148	10.0	165
1573	n/a		n/a	n/a	10.0	203	16.0	226

[a] Units are $\times 10^{-24}$ cm^2/(molecule-str). [b] Units are $\times 10^{-27}$ cm^2/(molecule-str). [c] Fermi doublet. [d] Vibronic mode.

Fermi doublet is in good agreement with experiment, due to the Franck−Condon activity of the fundamental.

Conclusion

We have implemented a procedure that employs calculated excited-state displacements along normal mode coordinates as inputs to the time correlator method for the prediction of resonance Raman intensities and frequencies. The procedure was applied to three molecules that serve as models for the aromatic amino acids tyrosine, phenylalanine, and tryptophan. The excited-state displacements corresponding to each normal mode frequency, ω_i, are expressed as electron−phonon constants, S_i, which were used as the inputs into the time correlator. The relatively good agreement of the calculated vibrational frequencies using *ab initio* and particularly DFT methods has been known for some time and has been confirmed here. However, the main focus of this work is the calculation of resonance Raman cross sections, which permits the prediction of Raman scattering intensities and calculation of REPs. The method gives reasonable agreement between calculated and experimental Raman cross sections for Franck−Condon active modes. Since the implementation of the time correlator is, at present, limited to A-term scattering of Franck−Condon active modes, vibrations that gain enhancement by pure B-term scattering had no calculated intensity. The Franck−Condon approximation was found to be largely valid for the $B_{a,b}$ transitions as expected for an allowed transition. However, the enhancement in resonance with $L_{a,b}$ transitions was also well represented by the calculated spectra since symmetry lowering by peripheral substituents greatly reduces the vibronic nature of these electronic transitions. Vibronic coupling is a reciprocal interaction between $B_{a,b}$ and $L_{a,b}$ transitions, which explains why it was possible to calculate the intensities of nontotally symmetric modes coupled to the $B_{a,b}$ transitions in relatively good agreement with experiment. The experimentally important Fermi resonances of tyrosine and tryptophan were also calculated in good agreement with experiment. These Fermi resonances have played a key role in the application of UV resonance Raman to monitor changes in protein structure in solution. Using the aromatic amino acids as an example, the present work validates a method based on excited-state potential energy surfaces of vibrational normal modes for the calculation of absolute resonance Raman cross sections.

Acknowledgment. We thank Dr. Bernard Delley for helpful discussions. We thank Dr. Andrew Shreve of Los Alamos

National Laboratory for providing the program TIMETHERM and for helpful discussions. We thank Dr. William Collier for the use of the program fcart01.

Supporting Information Available: Tables listing geometry changes in the excited state, graphs of excited-state potential energy surfaces used for normal mode displacements, vibrational mode depictions, comparison of calculated and experimental vibrational mode frequencies, calculated absorption spectra, potential energy distributions, combination band tables for *para*-cresol and 3MI, and complete sets of excitation profiles for all models. This material is available free of charge via the Internet at http://pubs.acs.org.

References and Notes

(1) Asher, S. A.; Ludwig, M.; Johnson, C. R. *J. Am. Chem. Soc.* **1986**, *108*, 3186.
(2) Cai, S. W.; Singh, B. R. *Biophys. Chem.* **1999**, *80*, 7.
(3) Eastman, J. W.; Sherwin, J. E.; Wong, R.; Liao, C. L.; Currier, R. J.; Lorey, F.; Cunningham, G. *J. Med. Screen.* **2000**, *7*, 131.
(4) Harada, I.; Miura, T.; Takeuchi, H. *Spectrochim. Acta, Part A* **1986**, *42*, 307.
(5) Johnson, C. R.; Ludwig, M.; Odonnell, S.; Asher, S. A. *J. Am. Chem. Soc.* **1984**, *106*, 5008.
(6) Lambert, S.; et al. *Organic Structural Spectroscopy*; Prentice-Hall Inc.: Upper Saddle River, NJ, 1998.
(7) McHale, J. L. *J. Raman Spectrosc.* **1982**, *13*, 21.
(8) Mikhonin, A. V.; Bykov, S. V.; Myshakina, N. S.; Asher, S. A. *J. Phys. Chem. B* **2006**, *110*, 1928.
(9) Spiro, T. G. *Acc. Chem. Res.* **1974**, *7*, 339.
(10) Tu, A. *Raman Spectroscopy in Biology*; John Wiley and Sons: New York, 1982.
(11) Fuson, N.; Garrigoulagrange, C.; Josien, M. L. *Spectrochim. Acta* **1960**, *16*, 106.
(12) Lord, R. C.; Miller, F. A. *J. Chem. Phys.* **1942**, *10*, 328.
(13) Wilson, E. B. *Phys. Rev.* **1934**, *45*, 0706.
(14) Peticolas, W. L.; Rush, T. *J. Comput. Chem.* **1995**, *16*, 1261.
(15) Sue, J.; Yan, Y. J.; Mukamel, S. *J. Chem. Phys.* **1986**, *85*, 462.
(16) Torii, H.; Tasumi, M. *J. Chem. Phys.* **1994**, *101*, 4496.
(17) Frisch, M. J.; Trucks, G. W.; Schlegel, H. B.; Scuseria, G. E.; Robb, M. A.; Cheeseman, J. R.; Montgomery, J. A., Jr.; Vreven, T.; Kudin, K. N.; Burant, J. C.; Millam, J. M.; Iyengar, S. S.; Tomasi, J.; Barone, V.; Mennucci, B.; Cossi, M.; Scalmani, G.; Rega, N.; Petersson, G. A.; Nakatsuji, H.; Hada, M.; Ehara, M.; Toyota, K.; Fukuda, R.; Hasegawa, J.; Ishida, M.; Nakajima, T.; Honda, Y.; Kitao, O.; Nakai, H.; Klene, M.; Li, X.; Knox, J. E.; Hratchian, H. P.; Cross, J. B.; Bakken, V.; Adamo, C.; Jaramillo, J.; Gomperts, R.; Stratmann, R. E.; Yazyev, O.; Austin, A. J.; Cammi, R.; Pomelli, C.; Ochterski, J. W.; Ayala, P. Y.; Morokuma, K.; Voth, G. A.; Salvador, P.; Dannenberg, J. J.; Zakrzewski, V. G.; Dapprich, S.; Daniels, A. D.; Strain, M. C.; Farkas, O.; Malick, D. K.; Rabuck, A. D.; Raghavachari, K.; Foresman, J. B.; Ortiz, J. V.; Cui, Q.; Baboul, A. G.; Clifford, S.; Cioslowski, J.; Stefanov, B. B.; Liu, G.; Liashenko, A.; Piskorz, P.; Komaromi, I.; Martin, R. L.; Fox, D. J.; Keith, T.; Al-Laham, M. A.; Peng, C. Y.; Nanayakkara, A.; Challacombe, M.; Gill, P. M. W.; Johnson, B.; Chen, W.; Wong, M. W.; Gonzalez, C.; Pople, J. A. *Gaussian 03*, Revision C0.2; Gaussian, Inc.: Wallingford, CT, 2004.
(18) Amos, R. D.; Rice, J. E. *Comp. Phys. Rep.* **1989**, *10*, 147.
(19) Pulay, P. *Mol. Phys.* **1969**, *17*, 197.
(20) Jensen, L.; Zhao, L. L.; Autschbach, J.; Schatz, G. C. *J. Chem. Phys.* **2005**, 123.
(21) Rappoport, D.; Furche, F. *J. Chem. Phys.* **2007**, 126.
(22) Jensen, L.; Schatz, G. C. *J. Phys. Chem. A* **2006**, *110*, 5973.
(23) Jensen, L.; Zhao, L. L.; Schatz, G. C. *J. Phys. Chem. C* **2007**, *111*, 4756.
(24) Delley, B. *J. Chem. Phys.* **1990**, *92*, 508.
(25) Shreve, A. P.; Mathies, R. A. *J. Phys. Chem.* **1995**, *99*, 7285.
(26) Lee, S. Y.; Heller, E. J. *J. Chem. Phys.* **1979**, *71*, 4777.
(27) Heller, E. J. *Acc. Chem. Res.* **1981**, *14*, 368.
(28) Johnson, C. R.; Ludwig, M.; Asher, S. A. *J. Am. Chem. Soc.* **1986**, *108*, 905.
(29) Ludwig, M.; Asher, S. A. *J. Am. Chem. Soc.* **1988**, *110*, 1005.
(30) Chen, X. G.; Asher, S. A.; Schweitzerstenner, R.; Mirkin, N. G.; Krimm, S. *J. Am. Chem. Soc.* **1995**, *117*, 2884.
(31) Asher, S. A.; Chi, Z. H.; Li, P. S. *J. Raman Spectrosc.* **1998**, *29*, 927.
(32) Rava, R. P.; Spiro, T. G. *J. Phys. Chem.* **1985**, *89*, 1856.
(33) Rava, R. P.; Spiro, T. G. *J. Am. Chem. Soc.* **1984**, *106*, 4062.
(34) Fodor, S. P. A.; Copeland, R. A.; Grygon, C. A.; Spiro, T. G. *J. Am. Chem. Soc.* **1989**, *111*, 5509.
(35) Hirakawa, A. Y.; Nishimura, Y.; Matsumoto, T.; Nakanishi, M.; Tsuboi, M. *J. Raman Spectrosc.* **1978**, *7*, 282.
(36) Mayne, L. C.; Hudson, B. *J. Phys. Chem.* **1991**, *95*, 2962.
(37) Mayne, L. C.; Ziegler, L. D.; Hudson, B. *J. Phys. Chem.* **1985**, *89*, 3395.
(38) Wen, Z. Q.; Thomas, G. J. *Biopolymers* **1998**, *45*, 247.
(39) Perdew, J. P.; Burke, K.; Ernzerhof, M. *Phys. Rev. Lett.* **1996**, *77*, 3865.
(40) Perdew, J. P.; Wang, Y. *Phys. Rev. B* **1992**, *45*, 13244.
(41) Delley, B. *J. Chem. Phys.* **2000**, *113*, 7756.
(42) Neese. ORCA, an ab initio density functional and semiempirical program package, University of Bonn, Germany, 2007.
(43) Library, T. b. s. ftp.chemie.uni-karlsruhe.de/pub/basen.
(44) Eichkorn, K.; Treutler, O.; Ohm, H.; Haser, M.; Ahlrichs, R. *Chem. Phys. Lett.* **1995**, *240*, 283.
(45) Eichkorn, K.; Weigend, F.; Treutler, O.; Ahlrichs, R. *Theor. Chem. Acc.* **1997**, *97*, 119.
(46) Collier, W. B. *J. Chem. Phys.* **1988**, *88*, 7295.
(47) Albrecht, A. C.; Hutley, M. C. *J. Chem. Phys.* **1971**, *55*, 4438.
(48) Hu, X. H.; Spiro, T. G. *Biochemistry* **1997**, *36*, 15701.
(49) Spiro, T. G. *Advances in Infrared and Raman Spectrsocopy*; University College: London, 1975; Vol. 1.
(50) Takeuchi, H.; Harada, I. *J. Raman Spectrosc.* **1990**, *21*, 509.
(51) Mix, G.; Schweitzer-Stenner, R.; Asher, S. A. *J. Am. Chem. Soc.* **2000**, *122*, 9028.
(52) Rava, R. P.; Spiro, T. G. *J. Phys. Chem.* **1985**, *89*, 1856.
(53) Chang, S.; Yang, W.; Spiro, T. G. *J. Raman Spectrosc.* **1990**, *21*, 435.
(54) Takeuchi, H.; Harada, I. *Spectrochim. Acta, Part A* **1986**, *42*, 1069.
(55) Takeuchi, H. *Biopolymers* **2003**, *72*, 305.

JP809431K